Münstermann, Sebastian; Wechsuwanmanee, Peerapon; Liu, Wenqi; Lian, Junhe

Surface roughness influences on localization and damage during forming of DP1000 sheet steel

Published in:
18th International Conference on Sheet Metal, SHEMET 2019, New Trends and Developments in Sheet Metal Processing

DOI:
10.1016/j.promfg.2019.02.168

Published: 01/01/2019

Document Version
Publisher's PDF, also known as Version of record

Available online at www.sciencedirect.com

ScienceDirect

Procedia Manufacturing 29 (2019) 504–511

Procedia MANUFACTURING

www.elsevier.com/locate/procedia

18th International Conference on Sheet Metal, SHEMET 2019

Surface roughness influences on localization and damage during forming of DP1000 sheet steel

Sebastian Münstermann[a]*, Peerapon Wechsuwanmanee[a], Wenqi Liu[a], Junhe Lian[b]

[a]*Integrity of Materials and Structures, Steel Institute, RWTH Aachen Uniuversity, Intzestraße 1, 52072 Aachen, Germany*
[b]*Engineering Materials, Department of Mechanical Engineering, Aalto Univerisity, Puumiehenkuja 3, 02150 Espoo, Finland*

Abstract

Surface roughness strongly influences the occurrence of edge cracks in metal forming processes. Recently, a sub-modelling approach has therefore been presented that is capable of predicting whether an edge forming process could be performed without failure events, but the macroscopic load-deformation behavior could not be predicted. This approach is extended to consider roughness induced micro damage even on the macroscopic scale. The concept is based on the idea to define an individual set of material parameters for those elements that are located at the sample´s surface. In order to calibrate the required set of parameters for these surface elements, sub-models are created which geometrically represent the roughness profiles that were determined experimentally before the bending tests were conducted. The procedure is demonstrated for the example of bending tests performed on samples made of steel DP1000 that have undergone two different surface treatments to adjust roughness conditions - fine grinding and polishing in the one extreme case and grinding with 80-grit sand paper in the other one. Experimental results reveal significant differences between the two sample configurations: while the samples with smooth surfaces remain free from cracks during the entire duration of the experiment, the samples with rough surfaces show fracture events. For both cases, the new simulation framework allows to reproduce both the macroscopic load-deflection curves and the individual damage and fracture behaviours.

Keywords: Surface Roughness; Strain Localization; Stress State Effects, Ductile Damage Accumulation

* Corresponding author. Tel.: +49-241-8092916; fax: +49-241-8092253.
E-mail address: sebastian.muenstermann@iehk.rwth-aachen.de

2351-9789 © 2019 The Authors. Published by Elsevier B.V.

10.1016/j.promfg.2019.02.168

Nomenclature

D	damage
DIL	damage initiation locus
DFL	ductile failure locus
DP	dualphase
E	elastic modulus
E_0	initial elastic modulus
E_{eff}	effective elastic modulus
FE	finite element
G_f	energy dissipation between damage initiation and ductile failure
MBW	modified Bai-Wierzbicki
$\bar{\varepsilon}^i$	equivalent plastic strain to damage initiation
$\bar{\varepsilon}^f$	equivalent plastic strain to ductile fracture
$\bar{\varepsilon}^p$	equivalent plastic strain
η	stress triaxiality
θ	Lode angle
$\bar{\theta}$	normalized Lode angle
Φ	yield potential
σ_e	equivalent stress
σ_m	mean stress
σ_{yld}	yield stress

1. Introduction

The edge crack sensitivity of advanced high strength steels is a severe obstacle for their application especially in the automotive industry [1]. Therefore, numerous scientific investigations have been carried out in the recent years aiming to understand the underlying mechanisms and influencing factors on edge crack sensitivity [2-5]. In general, the effects can be divided into two groups:

- Extrinsic influencing factors mainly resulting from the configuration of the edge manufacturing process.
- Intrinsic influencing factors resulting from the material´s microstructural configuration.

Microstructural impact on the edge crack sensitivity of multiphase steel is mainly given by inhomogeneous strain distributions resulting from mechanical property mismatch of the involved constituents [6]. This heterogeneity results in plastic strain concentration which most often activates damage initiation and accumulation mechanisms. A manufacturing process that involves local plastic straining can therefore leave a remarkable amount of residual ductile damage near the cutting zone, when multiphase steel with distinct property mismatch of the involved phases is processed.

The extrinsic influencing factors, on the other hand, have got a geometrical character. Every manufacturing process will leave its characteristic roughness profile on the manufactured surface, and this surface roughness obviously alters formability of sheet materials, since scratches and surface defects provoke strain localizations under less favorable stress states. Among others, the edge crack sensitivity of sheet materials can therefore be attributed to effects resulting from geometrical surface imperfections resulting from manufacturing.

Macroscopic constitutive models are typically not able to consider these effects, because surfaces are typically modelled smooth, and typical scratch depth is below the element edge length of the FE model [6]. Consequently, a scale-bridging simulation framework needs to be applied. Recently, an approach has been presented that applies sub-models containing geometrical surface information, so that damage initiation and accumulation could be quantified on the microscale, but no quantitative coupling back to the macroscopic scale could be achieved [6]. To solve this shortcoming is the aim of the present study.

In the studies depicted in [6], samples for VDA bending tests were manufactured from a dualphase steel of grade DP1000, but before the tests were conducted, the surfaces were treated systematically. Half of the samples were grinded and polished, whereas the other half was only grinded with 80-grit sand paper. During the experiments, the rough samples showed fracture events, whereas the smooth samples did not fail. Also, the measured load-deflection curves showed remarkable differences. In this paper, a simulation framework will be developed that is able to reproduce both load-deflection curves from a consideration of roughness profiles. To achieve this aim, the experiments are simulated with a ductile damage mechanics model with an individual set of material parameters for those elements that are located at the sample´s surface. In order to calibrate the required set of parameters for these surface elements, sub-models are created which geometrically represent the roughness profiles that were determined experimentally before the bending tests were conducted.

2. Material

For the study, a sheet steel of grade DP1000 was selected. The same material was also used for the study presented in [6]. Therefore, only a brief summary of the properties of this material is given here.

The chemical composition of the steel is presented in Table 1. The slim alloying concept is typical for this kind of steel grade, even though the Mn content is relatively high.

Table 1. Chemical composition of steel DP1000, mass content in %.

C	Si	Mn	P	Cr	Mo	Ni	Cu	N_{SS}
0.07	0.30	2.55	0.008	0.68	0.12	0.03	0.11	<0.0001

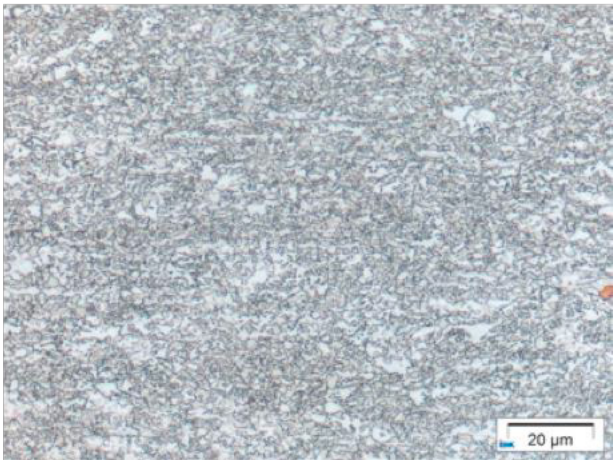

Fig. 1. Microstructure of steel DP1000

The material´s microstructure was quantitatively assessed by light optical microscopy. Samples for these investigations were carefully grinded, polished and etched with HNO_3. As shown by Fig. 1, the microstructure of the selected steel is composed of a ferritic matrix with dispersed islands of martensite. The fractions of ferrite and martensite are 62% and 38% respectively. A remarkable grain refinement strategy has been applied on the ferritic phase. Thereby, sufficient strength has been added to guarantee the required ultimate tensile strength of approximately1 GPa.

Strength properties were investigated with the help of tensile tests. These were conducted at isothermal, quasi-static conditions at room temperature. Samples for these tests were of the A_{80} geometry. The tests revealed a yield strength of 770 MPa, an ultimate tensile strength of 983 MPa, a uniform elongation of 5.2 % and an A_{80} fracture elongation of

11.0 %. Since the tensile test only covered a short part of the material´s flow curve, inverse FE analysis was conducted to find a reasonable flow curve approximation. After conducting this analysis, the following flow curve was identified, which mixes the approximations according to Swift and Voce:

$$\sigma_{\mathrm{yld}} = 0.5 \cdot 1300(2.3e^{-14} + \bar{\varepsilon}^{\mathrm{p}})^{\,0.075} + 0.5 \cdot \left[266.2 + 507.1\left(1 - e^{-73.94\bar{\varepsilon}^{\mathrm{p}}}\right)\right], \tag{1}$$

Samples for VDA bending tests [7] were created from this material for the investigations depicted in [6]. For these tests, two different surface conditions were adjusted: fine grinded and polished (smooth sample) or 80-grit sand paper grinded (rough samples). During the bending tests, the rough samples experienced fracture, while the smooth samples remained free from defects. The surface profiles were experimentally characterized by means of white light confocal microscopy. This information was later used to create the sub-models for surface representation.

3. MBW model

3.1. Model equations

The modified Bai-Wierzbicki (MBW) model applies the local approach to fracture, so that a clear indication of local conditions is required to properly apply the model. Since ductile fracture is well-known to be stress state dependent, one has to rely on parameters to characterize the state of stress which are derived from the three invariants of the stress tensor, namely the stress triaxiality and the Lode angle. With the principal stresses denoted by σ_1, σ_2 and σ_3, the three invariants of the stress tensor are defined respectively by

$$p = -\sigma_m = -\frac{1}{3}(\sigma_1 + \sigma_2 + \sigma_3), \tag{2}$$

$$q = \sigma_e = \sqrt{\frac{1}{2} \cdot [(\sigma_1 - \sigma_2)^2 + (\sigma_2 - \sigma_3)^2 + (\sigma_3 - \sigma_1)^2]}, \tag{3}$$

$$r = \left[\frac{27}{2} \cdot (\sigma_1 - \sigma_m)(\sigma_2 - \sigma_m)(\sigma_3 - \sigma_m)\right]^{\frac{1}{3}}, \tag{4}$$

Using these invariants, stress triaxiality and Lode angle can be calculated according to

$$\eta = -\frac{p}{q}, \tag{5}$$

$$\theta = \frac{1}{3} \cdot arccos\left[\left(\frac{r}{q}\right)^3\right], \tag{6}$$

While the influence of stress triaxiality on ductile fracture has been extensively described in literature [8-13], the consideration of the Lode angle is relatively new for plasticity and ductile fracture models [14-16]. For symmetry reasons, the Lode angle is defined for $0 \leqslant \theta \leqslant \pi/3$. By normalizing the Lode angle, the Lode angle parameter or normalized Lode angle is expressed by

$$\overline{\theta} = 1 - \frac{6\theta}{\pi}, \tag{7}$$

The presented studies initially rely on the MBW model as it was presented by Lian et al. [17]. This macroscopic ductile damage mechanics model takes the advantages of both the uncoupled and the coupled models. It makes use of a strain-based, stress-state dependent ductile damage initiation criterion which defines the equivalent plastic strain to ductile damage initiation as a function of stress triaxiality and normalized Lode angle. For strains lower than the damage initiation strain, no influence of damage on the material´s plastic reaction has to be considered, so that a conventional yield potential can be used in numerical simulations of sheet metal forming operations. On the other hand, once the damage initiation criterion is fulfilled, the damage-induced softening has to be considered. For this purpose, a damage variable is coupled into the yield potential, and a corresponding damage evolution law has to be given. The MBW model has been strongly inspired by an uncoupled ductile fracture model initially proposed by Bai and Wierzbicki [18]. With the suggested modifications, especially the damage initiation criterion, the multiscale characterization of both damage and fracture can be achieved. The MBW model describes isotropic hardening whilst neglecting any kinematic hardening. With the equivalent stress denoted as σ_e, the yield stress denoted as σ_{yld} and the ductile damage variable denoted as D, its yield potential reads:

$$\phi = \sigma_e - (1-D)\sigma_{yld} \leq 0, \tag{8}$$

The MBW model applies the effective stress concept, so that the damage variable is also applied on the elastic material constants. With the initial Young´s Modulus E_0 and the effective Young´s Modulus E_{eff}, the concept reads:

$$E_{eff} = (1-D)E_0, \tag{9}$$

The so-called damage initiation locus (DIL) defines the onset of ductile damage in the MBW model. It defines the equivalent plastic strain at ductile damage initiation. Since this parameter shows a pronounced sensitivity on the local state of stress, it is formulated as a function of the stress triaxiality and the normalized Lode angle:

$$\bar{\varepsilon}^i = \left(c_1^i \cdot exp\left(-c_2^i \cdot \eta\right) - c_3^i \cdot exp\left(-c_4^i \cdot \eta\right)\right)\bar{\theta}^2 + c_3^i \cdot exp\left(-c_4^i \cdot \eta\right), \tag{10}$$

Note that all “c” parameters with upper and lower indices are material parameters that have to be fitted to experimental data. In order to characterize the failure of a material point, the ductile failure locus (DFL) is defined as presented by eq. 11. Moreover, a linear relationship between the damage variable D and the equivalent plastic strain is assumed for strains between the ductile damage initiation locus and the ductile failure locus. Its slope is characterized by the characteristic energy dissipation G_f.

$$\bar{\varepsilon}^f = \left(c_1^f \cdot exp\left(-c_2^f \cdot \eta\right) - c_3^f \cdot exp\left(-c_4^f \cdot \eta\right)\right)\bar{\theta}^2 + c_3^f \cdot exp\left(-c_4^f \cdot \eta\right) \tag{11}$$

The MBW model is implemented as a user-defined material model in terms of a VUMAT for Abaqus/Explicit. It is embedded into the framework of the small strain concept. In case the model is applied in the finite strain plasticity, the kinematic transformations are performed first. Then, the constitutive equations governing the finite deformation are formulated using strains and stresses and their rates defined on an unrotated frame of reference. Likewise, the stress updating procedure remains as it was for the small strain formulation. Abaqus adopts this kind of treatment for finite strain plasticity, so that only the small strain theory needs to be considered when user material subroutines are created for this FE solver.

3.2. Parameter calibration

The conventional strategy of parameter identification for the MBW model relies on an iterative procedure. It is based on the idea to find one set of material parameters that allows to describe the constitutive behavior of the material under different states of stress. In order to systematically adjust the state of stress, different sample geometries are investigated. Typical examples for these different geometries are notched dog bone samples, notched plane strain samples, and central hole samples. Fig. 2 shows experimental force-elongation curves for this material together with the corresponding MBW model predictions after successful parameter calibration.

During the parameter identification it could be revealed that the DIL and the DFL nearly fall together for the steel DP1000. It means that the failure behavior of this material is characterized by late damage initiation and rapid damage accumulation. For reasons of simplicity, the material behavior can therefore be characterized by the damage initiation locus alone. Its parameters as well as all further MBW parameters are summarized in table 2.

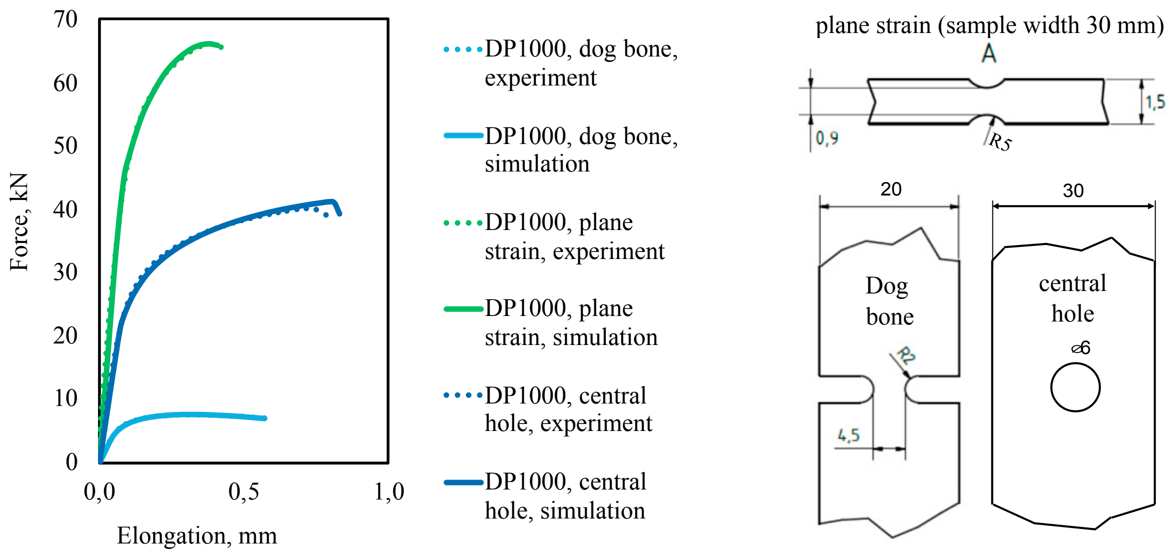

Fig. 2. Force-elongation curves from experiment and MBW model prediction for different sample geometries depicted on the right side.

Table 2. MBW model parameters

c_1^f	c_2^f	c_3^f	c_4^f	G_f
1.24	3.0	0.29	0.78	2500

4. Reproduction of failure criteria for surface elements

The strategy to incorporate surface roughness effects into failure predictions is based on the idea to define artificial MBW parameters for all elements located at the surface of the sample, while all remaining elements still rely on the initial set of parameters. Compared to the previous work summarized in [6], this is a new approach, which will allow to capture roughness effects even on the macroscopic scale. Nevertheless, its superior prediction quality will be demonstrated based on the already existing set of experimental results.

Fig. 3. Sub-models with geometrical surface representation

First of all, the roughness profiles were used to create the sub-models depicted in Fig. 3 [6]. Afterwards, the sub-models were meshed and loaded with plane strain boundary conditions. These were selected because failure during VDA bending tests is also triggered under plane strain conditions. For the simulations of the sub-models, the MBW model was employed. Simulations were stopped when elements in a process zone of 5µm x 5 µm had reached the DFL. This value was chosen because it reflects the typical void size that is characterized by the damage initiation locus when applied on the mm scale. Afterwards, for the same displacement a model with smooth surface was evaluated with respect to the equivalent plastic strain. As expected, due to the missing strain consideration resulting from surface roughness, the strain level in the “smooth model” was significantly lower. Finally, this lower level was considered as limit strain for the surface elements. In order to construct the full ductile fracture locus for the surface elements, the ratio between failure strain of the rough and the smooth configuration was assumed to be constant.

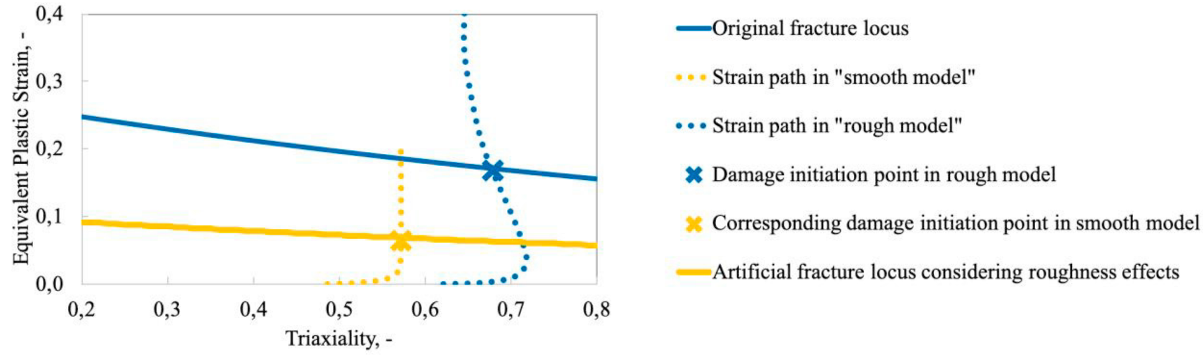

Fig. 4. Calibration of the artificial fracture locus of steel DP1000.

Fig. 4 exemplarily shows this procedure. The illustration shows a diagram in which equivalent plastic strain is plotted over stress triaxiality. The original fracture locus is plotted as a hyperbolic function for the plane strain condition, and the strain path as it is calculated with the "rough" model representing the 80-grit sand paper grinded condition is also depicted. At the intersection between the two blue curves, damage is triggered in the rough model. A smooth model (orange curve) would have experienced significantly smaller equivalent plastic strain for the loading conditions that have been identified as critical for the rough model. Noteworthy, also the stress state is slightly different. In order to predict the onset of damage and fracture in a rough sample without geometrical representation of the roughness profile, therefore the artificial fracture locus (depicted in orange) should be used. In total, it turns out that the influence of roughness is rather significant in the present example.

5. Application to bending tests

The VDA bending tests performed for the investigations depicted in [6] were simulated with the MBW model. For all elements situated in the bulk, the original set of MBW model parameters was used, whereas for surface elements, the artificial parameter set was used that considers roughness effects. Fig. 5 [7] gives the geometrical set-up of the test. The roller distance in the tests was 6 mm, whereas the roller diameter was 18 mm. Rectangular samples with a length of 60 mm, a width of 20 mm and a thickness of 1.5 mm (initial thickness) were investigated in the two abovementioned surface conditions. The experiments were conducted until the specimens started slipping along the rollers. For the smooth samples, this happened at a punch displacement of approximately 12 mm [6].

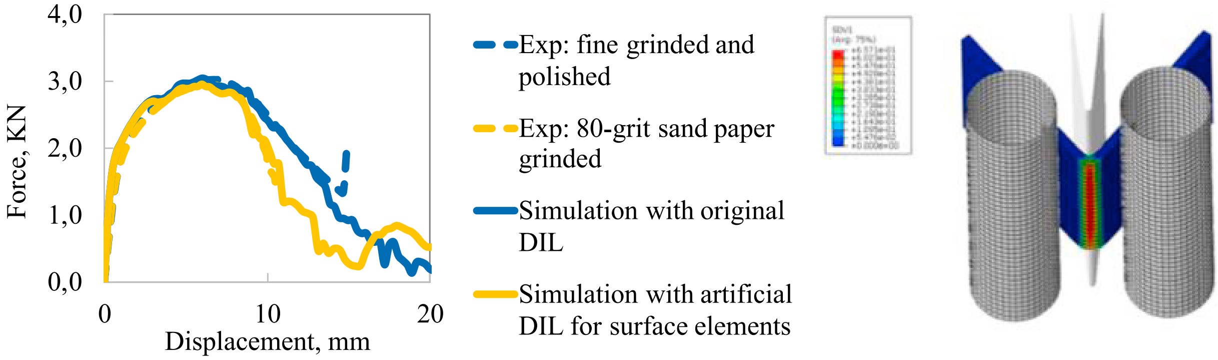

Fig. 5. Force-displacement curves for VDA bending tests from experiment and MBW simulation (left side). Distribution of equivalent plastic strain in the bending sample simulated with a mesh size of 0.1 mm (right side).

The numerical simulations were performed in Abaqus/Explicit with a user defined material model established as VUMAT. The samples where meshed as brick elements with an edge length of 0.1 mm. The same mesh size was also applied during the simulations of central hole tests, notched dog-bone tests and notched plane strain tensile tests in order to minimize mesh size effects. Fig. 5 presents a comparison of force-displacement curves from experiment and simulation for both surface conditions. It turns out that with the presented approach, the influence of surface roughness can even be numerically described on the macroscopic scale, even though the consideration lies only in the set of material parameters.

6. Conclusions

Extrinsic and intrinsic influencing factors alter the edge formability of multiphase steel. With the presented approach, the effect of extrinsic factors can be quantitatively assessed. This provides the opportunity to better interpret experimental results of hole expansion tests that were derived for one material after different manufacturing processes. The results show that a consideration of roughness effects on the material parameter level is sufficient to quantitatively evaluate the effect of surface imperfections on the macroscopic load-deformation behavior. This implies that it is not necessary to investigate these factors on the geometrical level in macroscopic simulations. Since this task would be very harmful for the computational efficiency, the suggested simulation framework can be very beneficial for the computational costs for the future.

References

[1] A. Ilinich, L. Smith, S. Golovashchenko, Analysis of Methods for Determining Sheared Edge Formability, SAE Technical Paper, (2011) 2011-01-1062.
[2] I. Tsoupis, S. Hildering, M. Merklein, Bending of high-strength low-alloyed steel with respect to edge crack sensitivity caused by shearing operations Procedia Engineering, 81 (2014) 712-717.
[3] Q.B. Le, J.A.deVries, S.F. Golovashchenko, J.J.F. Bonnen, Analysis of sheared edge formability of aluminum, Journal of Materials Processing Technology, 214 (2014) 876-891.
[4] C. Ye, J. Chen, C. Xia, X. Yu, Study of curvature and pre-damage effects on the edge stretchability of advanced high strength steel based on a new simulation model, International Journal of Material Forming, 9 (2016) 269-276.
[5] N. Habibi, F. Pütz, M. Könemann, V. Brinnel, S. Münstermann, M. Feistle, W. Volk, Numerical quantification of damage accumulation resulting from blanking in multi-phase steel, IOP Conf. Ser.: Mater. Sci. Eng., 418 (2018) 012058.
[6] S. Münstermann, P. Wechsuwanmanee, W. Liu, J. Lian, A numerical approach to evaluate roughness effects on localization and damage in sheet materials, IOP Conference Series.: Materials Science and Engineering, 418 (2018) 012038.
[7] VDA 238-100 (test specification), Plate bending test for metallic materials, Verband der Automobilindustrie E. V. (VDA), Berlin, Germany.
[8] F.A. McClintock, A criterion of ductile fracture by the growth of holes, Journal of Applied Mechanics, 35 (1968) 363–371.
[9] J.R. Rice, D.M. Tracey, On the ductile enlargement of voids in triaxial stress fields, Journal of the Mechanics and Physics of Solids, 17 (1969) 201–217.
[10] J.W. Hancock, A.C. Mackenzie, On the mechanisms of ductile failure in high-strength steels subjected to multi-axial stress-states, Journal of the Mechanics and Physics of Solids, 24 (1976) 147–160.
[11] A.C. Mackenzie, J.W. Hancock, D.K. Brown, On the influence of state of stress on ductile failure initiation in high strength steels, Engineering Fracture Mechanics, 9 (1977) 167–168.
[12] G.R. Johnson, W.H. Cook, Fracture characteristics of three metals subjected to various strains, strain rates, temperatures and pressures, Engineering Fracture Mechanics, 21 (1985) 31–48.
[13] Y. Bao, T. Wierzbicki, On fracture locus in the equivalent strain and stress triaxiality space, International Journal of Mechanical Sciences, 46 (2004) 81–98.
[14] I. Barsoum, J. Faleskog, Rupture mechanisms in combined tension and shear—experiments, International Journal of Solids and Structures, 44 (2007) 1768–1786.
[15] X. Gao, G. Zhang, C. Roe. A study on the effect of the stress state on ductile fracture. International Journal of Damage Mechanics 19 (2009) 75–94.
[16] G. Mirone, A new model for the elastoplastic characterization and the stress–strain determination on the necking section of a tensile specimen, International Journal of Solids and Structures, 41(2004) 3545–3564.
[17] Y. Bai, T. Wierzbicki, A new model of metal plasticity and fracture with pressure and Lode dependence, International Journal of Plasticity, 24 (2008), 1071–1096.
[18] J. Lian, M. Sharaf, F. Archie, S. Münstermann, A hybrid approach for modelling of plasticity and failure behavior of advanced high-strength steel sheets, International Journal of Damage Mechanics, 22 (2013) 188 - 218.